Type of contribution:
Editorial
▶ Research Paper
Case Study
Review Paper
Scientific Data
Report of Tech. Application

e-issn. 2798-5245

Mechanical Engineering for Society and Industry
Vol. 1, No. 2 (2021) pp 86-95
https://doi.org/10.31603/mesi.5903

Emphasis of Weld Time, Shielding Gas and Oxygen Content in Activated Fluxes on the Weldment Microstructure

Surinder Tathgir[1], Dinesh W. Rathod[2]*, Ajay Batish[1]

[1] Department of Mechanical Engineering, Thapar Institute of Engineering & Technology, Thapar Technology Campus, Patiala–147004, **India**
[2] Department of Mechanical Engineering, National Institute of Technology Srinagar, Hazratbal, Srinagar–190006, **India**
✉ dinesh.rathod@nitsri.ac.in

This article contributes to:

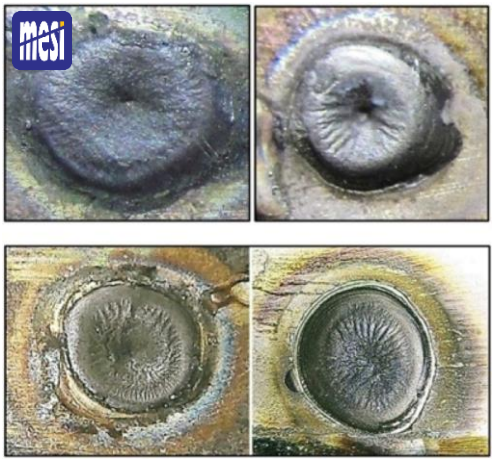

Highlights:

- Welding time, shielding gas and oxygen in active flux on the welding microstructure were studied
- The oxygen content of the oxide-based active flux provides extra heat during flux decomposition
- The use of a hydrogen mixed shielding gas has a significant impact on the welding result
- The ferrite and austenite grain growth as well as the dendrite arm spacing found to be increased due to H_2 in shielding gas

Abstract

The activated-TIG (A-TIG) process is a recognised process for achieving higher depth-of-penetration (DoP) and it could be used for various stainless-steel grades welding. The oxygen content of oxide based activated fluxes provide the extra heat during decomposition of flux and result into deep penetration. This study reveals the effect of short weld time of 2 sec in stationary arc, shielding environment (Ar and Ar + 2.5 % H_2) and an effect of oxygen element in activated flux (CrO_3 and SiO_2) on the microstructure and weld metal micro-hardness. Use of hydrogen mix shielding gas during A-TIG process has significant impact on the dilution rate, grain size and dendrite arm spacing. The fraction of oxygen in the flux and the presence of silicon in SiO_2 flux play a significant role in achieving higher DoP. To evaluate the impact of different shielding environment on grain growth, the samples were investigated with weld pool morphology, depth of penetration, weld chemistry, optical microscopy and SEM analysis. The extra heat produced due to oxygen fraction in activated flux and H_2 induced shielding have been quantified in the study. The ferrite and austenite grain growth as well as the dendrite arm spacing found to be increased due to presence of H_2 in shielding gas.

Keywords: Short weld time, Reverse marangoni, Hydrogen, Grain growth, Dendrite arm, Electron attachment, Oxygen rich elements

Article info
Submitted: 2021-09-22
Revised: 2021-09-30
Accepted: 2021-10-06

Publisher
Universitas Muhammadiyah Magelang

1. Introduction

Duplex stainless steel (DSS) is one of the stainless steel type, which have two phases (austenite and ferrite) in its microstructure in approximately equal amount [1]. This two phase structure helps to maintain the unrivalled mechanical properties at low level temperature to elevated temperature which further makes its use in nuclear power plants, offshore structures and oil extraction industries [2]. Many variants of conventional Gas Tungsten Arc Welding (GTAW) or Tungsten Inert Gas (TIG) process (DP-TIG, K-TIG) are used for the welding of austenitic stainless steel (ASS) and duplex stainless steel (DSS) [3], [4].

Activated GTAW or A-TIG welding is a modified version of conventional GTAW which has the characteristics of inward flow of liquid metal (Reversed Marangoni Convection) under the influence of activated fluxes. The welding quality is strongly characterized by the weld bead geometry and its associated weldment microstructure. The factors responsible for the resulted microstructure are the heat input [5], welding time or speed, shielding gases and type of activated flux.Depth of penetration (DoP) is a significant factor in TIG welding and the weld bead geometry plays a vital role in determining the strength of the weld [6]. Typical issues associated with conventional TIG are its low productivity, as it requires significant attention for achieving good quality welded joints and hence, thereby hampering a higher production rate. To overcome the limitation A-TIG is found to be significant welding technique as a variant of GTAW. In this welding technique the most prominent effect on penetration is influenced by the Lorentz force and occurrence of reverse Marangoni convection. The combined effect of Lorentz force and reverses Marangoni convection, which affects change the distribution of charge carrier by changing the behaviour of ions and electrons during welding [7]–[10]. Higher DoP during TIG welding can be possible through A-TIG welding [8], [11].

To achieve higher DoP and increasing productivity of the TIG welding, argon is mixed with other gases like hydrogen and helium with varying percentages. The thermal conductivity of H_2 and He gas is higher than Ar gas, So the addition of these gases increases the arc temperature, which result in higher DoP [9], [12]. Another reason of higher DoP in case of A-TIG welding is occurrence of reverse Marangoni convection, when the gradient of surface tension changes from negative to positive during decomposition of flux metallic compound [8]–[10]. Marangoni convection occurs when weld metal oxygen content reaches above 70×10^{-6} [13].Activated fluxes like SiO_2, MoO_3, and $Cr2O_3$ are reported [14] with improved penetration and mechanical properties of Duplex 2205 stainless steel welds while comparing it to the conventional TIG welds [2]. Presence of oxygen after decomposition of fluxes (oxygen based) also plays a vital role by attaching electronsand formation of negative ion to the outer region of arc [15] result into arc constriction behaviour which could further increase the heat energy density of arc, reduction of anode root area and hence result into higher weld pool temperature [15]. The higher temperature produce more molten metal which further increase the overall dilution rate [10], [16]. The diffusion of elements is fully dependent on the heat generation in the weld pool [17]. The oxide based fluxes also act as an insulator barrier to the flow of current and for the outer region for the arc, which in result increases the magnetic pinching effect due to higher current density of the central part of the arc and it favours the downward flow of molten metal [18], [19].

2. Objectives

The present study investigated an effect of short duration weld time of two seconds (2 s) for A-TIG welding under Ar and Ar + 2.5% H_2 shielding environment on the microstructure. Change in dendrites spacing and size and grain growth due to fluxes and the shielding environments have been discussed and compared. The distinctive observations with associated mechanism are elaborated in the present study for better understanding of the mechanism during short welding time.

3. Material and Experimental Procedure

In this study, Duplex stainless-steel of 2205 type with 5 mm thickness was used to find the effect of oxide based activated flux (CrO_3 and SiO_2) which had a purity of 99 % and 99.5 % under the Ar and Ar + 2.5% H_2 shielding environment. The chemical composition of as received Duplex-2205 steel was checked by Optical emission spectroscopy (Make: Foundry Master, Germany) is given in Table 1.

The average value from the three measurements has been used for the analysis in this study. All weld coupons were cut from a flat plate and before welding, they were cleaned for oxide free surface by grinding and acetone cleaning. The oxide base fluxes like CrO_3, and SiO_2 were used in the form of thin paste (mixed with acetone) layer and that is applied on the substrate plates. The complete dried layer of paste was ensured before A-TIG welding. In spite of stringer (straight) bead, a stationary arc (at a spot) method was used [10] for identifying the effect of shielding environment and change in number of oxygen elements of activated flux on the microstructure in terms of grain growth, weld profile, mode of heat transfer, dilution rate and other weld metal properties. A-TIG welding was employed using 150 *Amp* (*A*), 10 volts (*V*) using Ar and mixture of Ar

+ 2.5% H_2 gas with 10 *L/min* gas flow rate. A standard gap of 3 mm was maintained between electrode and the job during all the experiments.

The top surfaces of as-welded A-TIG weld coupons under Ar and Ar + 2.5 % H_2 shielding with the schematic of A-TIG process is shown in Figure 1. The extracted specimens from the weld coupons were polished and etched with carpenter etchant for further study Optical Microscopy (DMILM, make: Leica), Scanning electron microscopy (SEM - JEOL_JSM_6510LV), and micro-hardness (Metatech_MVH-1) tests. The weld bead profiles were measured using optical microscope and the micrograph analysis was done by Image - J software.

Table 1. Chemical Compositions of Duplex-2205

Material	Percentage Composition (% wt.)											
	C	Mn	Si	Cr	Ni	S	P	Mo	Cu	W	Nb	Fe
Duplex 2205 steel	0.03	1.8	0.38	25.1	4.68	0.005	0.02	3.08	0.18	0.02	0.002	Bal

4. Results and Discussion

4.1. Arc constriction phenomena of A-TIG welding

The TIG welding arc has a sufficient temperature to melt the oxide layer/activated flux within a short duration time. Under the intense heat of arc, the activated flux decomposes however some of the excessive flux converted into slag (that not consumed in reaction). This unconsumed slag can be visible around the weld spots (Figure 1). Under the intense heat of arc, the flux which contains metallic oxides decomposes to produce some oxygen. This oxygen gas helps in electron attachment with the outer region of the arc to form negative ion which further leads to arc constriction and increase in current density. The mechanism of decomposition, electron attachment and detachment of negative ions could be analysed from the following reactions:

$$4CrO_3 = 2CrO_3 + 3O_2 \quad (1) \quad [10]$$

$$3CrO_2 = 3Cr + O_3 \quad (2) \quad [10]$$

$$2O_3 + 3e = 3O_2^- \quad (3)$$

$$O_2 + e = O_2^- \quad (4)$$

$$O_2^- + M \rightarrow e + O_2 + M \quad (5) \quad [15]$$

Similarly, in case of SiO_2

$$(SiO_2) = SiO(g) + ½\ O_2\ (g) \quad (6) \quad [10]$$

$$SiO\ (g) = Si + O \quad (7) \quad [10]$$

$$SiO + e = Si + O^- \quad (8)$$

In the present case, the silicon could have high affinity towards the electrons, and that could be the principle reason of enhanced dilution in case of SiO_2 flux. The arc constriction behaviour can reduce the anode root area with an increase ofenergy density. This significant increase in the concentrated energy density may further increases the melting rate and the overall dilution rate.

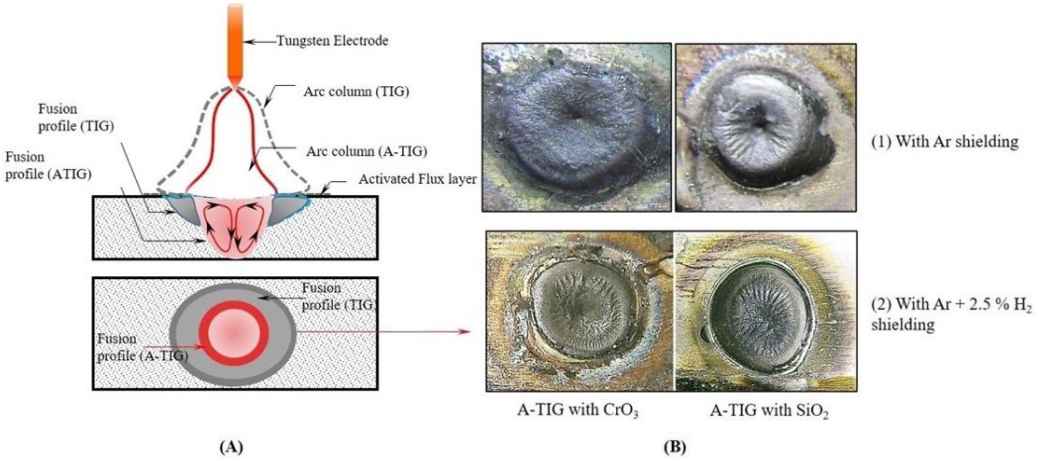

Figure 1. (A) Schematic representation of stationary arc of A-TIG welding (B) Weld surface appearance

4.2. Change in surface tension gradient

Another associated mechanism for the deeper penetration in case of A-TIG welding is the occurrence of reverse Marangoni convection [20]. In particular case of A-TIG welding, the change

in the surface tension gradient (dγ/dT) i.e. from negative to positive with increase of temperature causes the reverse convective flow of liquid metal from radially outward to radially inward [7], [21]. Due to this reverse convective flow of liquid metal higher DoP is achieved. Hence, A-TIG welding create funnel type cavity.

4.3. Weld pool morphology

From the microstructure, in Figure 2 the epitaxial growth of both ferrite and austenite dendrite is clearly visible. The dark phase represents to ferrite with white arrow and the light phase represent the presence of austenite phase with yellow arrow. The concentration of delta ferrite matrix is uniformly distributed in the microstructure. The dendrite growth direction in case of Ar + 2.5 % H_2 shielding is almost vertical ~0-to-5°. However, in case of pure Ar shielding the angle of dendrite growth has been noticed at ~45° with weld centreline. This noticeable directional feature of microstructure is due to the change in cooling rate. The elements like oxygen and silicon in activated fluxes are expected to participate in weld pool reactions and that leads to the variable weld pool behaviour by means of metal flow pattern associated with the reverse Marangoni convection.

By considering Figure 2, it is observed that the effect of reverse Marangoni is found more in case of SiO_2 samples due to presence of silicon. As silicon has greater affinity towards electrons because Silicon (Si) have more electronegativity [22] which results in a concentrated constricted arc and hence, it may cause to deep penetration as compare to CrO_3 flux (Figure 3). Moreover, the higher current density helps to ionize more Ar atoms, which finally increases the ionization of arc plasma and enhanced arc energy. So, the deeperpenetration happened in case of Ar shielding compared to the Ar + 2.5 % H_2 [16] shielding.Presence of H_2 in Ar gas increases the arc energy but due to short weld- time (2 s) available to react it may not change the flow of liquid metal in the radially inward direction.Moreover, the flow of liquid metal was found in radially outward direction, which increased the width of weld. The presence of such a reactive gas for the short duration results into significant increase in the width of weld pool in both activated fluxes. The instance of wider weld beads can be noticed from Figure 3.

4.4. Effect of H_2 on heat energy produced

In accordance to the macrostructures analysed in Figure 2 and their corresponding weld bead profile in Figure 3, the dilution area of CrO_3 fluxed weld coupon of Ar and Ar + 2.5 % H_2 shielding was measured as 17.62 mm^2 and 18.92 mm^2. Similarly, the dilution area for SiO_2 welded samples of Ar and Ar + 2.5 % H_2 shielding was measured as 19.61 mm^2 and 20.01 mm^2. A significant difference in the overall dilution rate is found in case of CrO_3 and SiO_2 welded sample in terms of melting area/dilution area and it is found in agreement with M. Suban et. al. [16] where, melting rate increases with the small addition of H_2. The heat energy is measured in watt (*W*) [10] where, the heat energy (*V* * *I*) has been estimated to the 1500 *W* in accordance with the process parameters used in present study. Hence, the energy needed for the dilution in case of CrO_3 flux weld samples of Ar and Ar + 2.5 % H_2 shielding is 85.13 *W* and 79.28 *W* and that suggests the lesser energy requirement in given dilution owing to presence of H_2 in Ar gas. Similarly, in case of SiO_2 flux weld samples of Ar and Ar + 2.5 % H_2 shielding, the energy required is 76.49 *W* and 74.96 *W* respectively. However, the difference between the energies in case of SiO_2 is only 1.53 *W*, which is quite less compared to CrO_3 flux welded samples. This is observed be due the presence of more oxygen content in CrO_3 flux to react with the H_2 in case of H_2 mixed shielding gas.

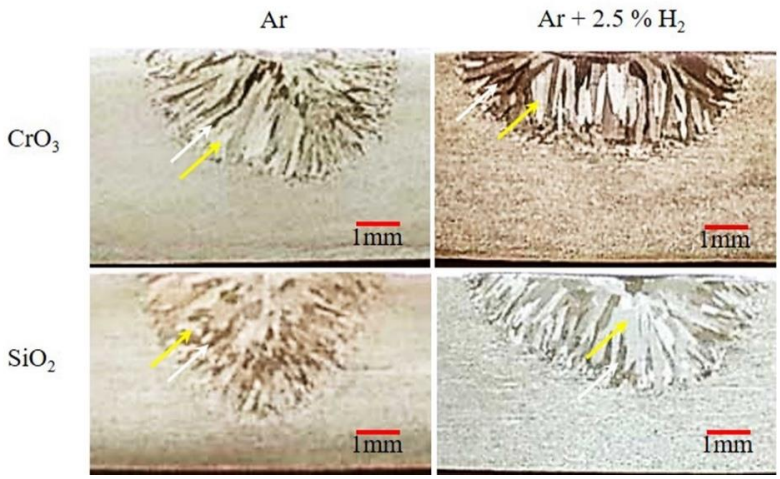

Figure 2. Macrostructure of A-TIG welded samples under Ar and Ar + 2.5 % H2 shielding

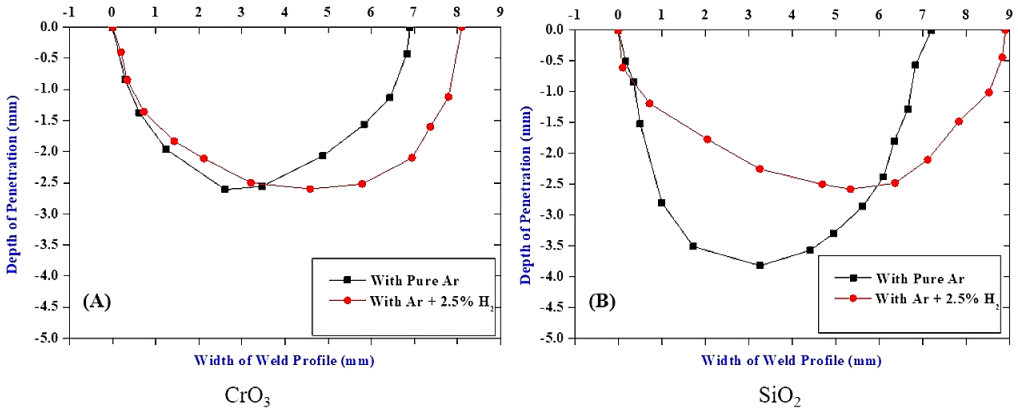

Figure 3. Weld bead profile of CrO_3 and SiO_2 weld couponsunder Ar and Ar + 2.5 % H2 shielding

4.5. Solidification and dendrite growth in weld centre

The solidification of weld metal and the dendrite growth is strongly influenced by the thermal gradient. Due to more oxygen content available in CrO_3 flux and presence of hydrogen in the shielding environment leads to more dendrite growth in the weld centre / fusion zone. The general structure of weld centre of CrO_3 and SiO_2 is shown in Figure 6, A – D represents the microstructure for CrO_3 and SiO_2 fluxed weld metal. The mixed mode of ferritic-austenite structure revealed in all specimens. The general structures are not notice with the presence of significant carbide or second phase precipitates. The presence of Widmanstatten austenite from the boundary of ferrite grain in the form of needles can be seen in case of SiO_2 flux welded sample under the mixed shielding environment, which justified the presence of secondary austenite. Whereas in case of Ar shielded environment the austenite is distributed in small pallets in ferrite grains of the sample welded with SiO_2 flux. A well-defined growth of both phases dendrites is also visible in case of mixed shielding environment as compared to pure Ar environment due to higher temperature under hydrogen shielding environment. The size of dendrite arms spacing is significantly varied in each flux condition. The dark brown shade represents the presence of ferrite phase and the white shade represent the presence of austenite phase in the macrostructure of Figure 6.

In mixed shielding environment i.e. Ar + 2.5% H_2 (Figure 4 C and Figure 4 D) the average ferrite dendrite arm spacing (AFDAS) and average austenite dendrite arm spacing (AADAS) in the weld centre of 2 sec arc exposure time for CrO_3 welded sample are measured as 100 µm and 80 µm. Whereas in case of SiO_2 welded sample the ferrite dendrite arm spacing (FDAS) and austenite dendrite arm spacing (ADAS) was measured as 80 µm and 50 µm. However, for pure Ar shielding environment the average ferrite dendrite arm spacing (AFDAS) and average austenite dendrite arm spacing (AADAS) in the weld centre of CrO_3 welded sample are measured as 80 µm and 60 µm. Whereas in case of SiO_2 welded sample the ferrite dendrite arm spacing (FDAS) and austenite dendrite arm spacing (ADAS) was measured as 60 µm and 56 µm. The cooling rate (G x R) is higher in the centre axis of weld pool and lower at the boundary of fusion line. This may suggest that the dendrite arm spacing decreases from the fusion boundary to the centre part because the dendrite arm spacing decreases with increasing of cooling rate (G x R).

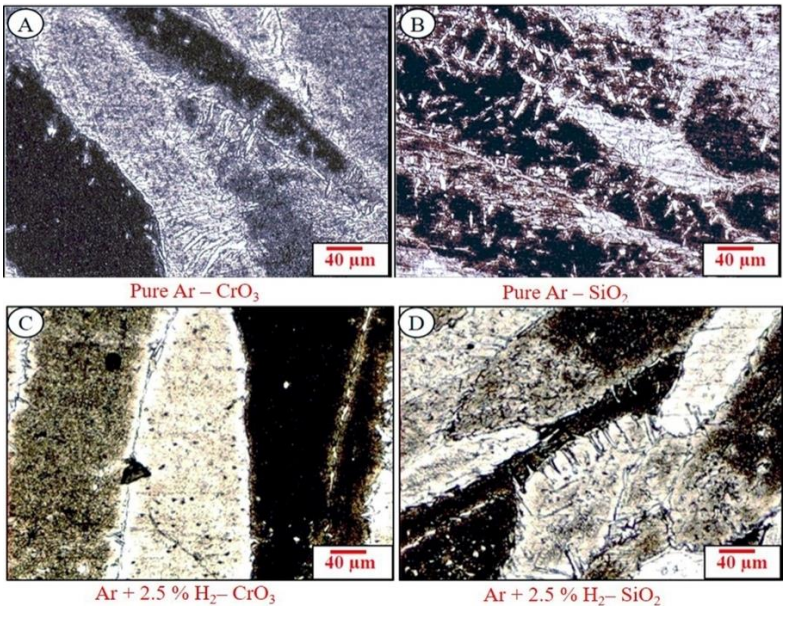

Figure 4. Optical microstructure of weld centre under Ar and Ar + 2.5 % H_2 shielding

4.6. Solidification and grain growth in HAZ

The occurrence of the grains depends on free energy (***ΔG****). When it has a negative value then a transformation occurs spontaneously and when the cluster reaches to the critical radius i.e. ***r**** then growth will continue with accompaniment of free energy. The interface of HAZ and the parent metal shows the dendrite growth direction or the epitaxial growth in Figure 5. From the epitaxial growth at the interface, it could be analysed that the amount of austenite precipitation is more in the HAZ in case of SiO_2 welded samples for Ar shielding (Figure 5) whereas inCrO_3 welded sample the more amount of ferrite phase precipitation is visible in left hand microstructure. Coarse grains are found in both the microstructures.

However, in case of SiO_2 welded sample, the growth of ferrite is more under Ar shielding environment. Whereas for Ar + 2.5 % H_2 shielding more ferrite dendrite appears after solidification in CrO_3 welded sample (Figure 6). The reason behind ferrite growth is due to reaction of H_2 with excess present oxygen content in CrO_3 flux, which may lead to attain higher temperature of the weld pool. The epitaxial solidification of the grains from the base grains has been found more in the case of a hydrogen mixed environment as compared to a pure Ar shielding environment [12]. The thickness of HAZ, approximately 50µm has been found less in the mixed shielding environment. The temperature gradient (G) and growth rate (R) with associated ratio of (G/R) and the product of G x R may influence the average dendrite size and average dendrite arm spacing [23], [24].

The austenite grain size (AGS) and the ferrite grain size (FGS) for parent metal was observed to be ~34 micron (ASTM E112-96 number – G 6.5 – 7) and ~20 micron (ASTM E112-96 number – G 8 – 8.5). For the comparison of grain growth in heat affected zone (HAZ), the grain size of parent metal has been compared. The growth of austenite and ferrite grains in HAZ is fully dependent on the generation of heat due to activated flux and the shielding gas. The average growth of austenite grain size (AGS) in HAZ of Ar shielding environment for CrO_3 flux has been found as ~28 micron (G7 – 7.5) and in Ar + 2.5 % H_2 shielding it was measured as ~50 micron (G5.5 – 6). Whereas, growth average of ferrite grain size (FGS) for CrO3 flux in Ar gas shielding was observed as ~40 micron (G6 – 6.5) and in case of Ar + 2.5 % H_2 shielding it was measured as ~42 micron (G6 – 6.5).

However, in case of SiO_2 flux the average growth of AGS observed as ~25 micron (G7.5 – 8) in both the shielding environment. Whereas, average growth of FGS for SiO_2 flux in case of Ar shielding was observed as ~40 micron (G6 – 6.5) and in Ar + 2.5 % H_2 shielding it was measured as ~45 micron (G5.5 – 6).

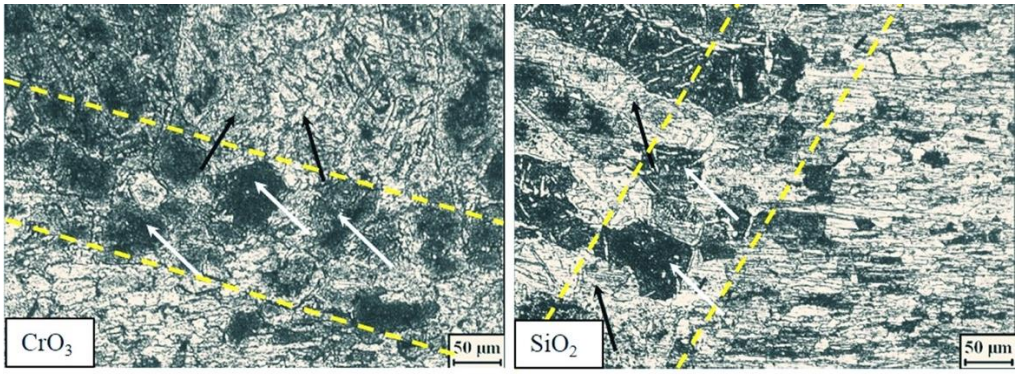

Figure 5. Optical micrograph of A-TIG welded samples with CrO_3 and SiO_2 flux under pure Ar shielding

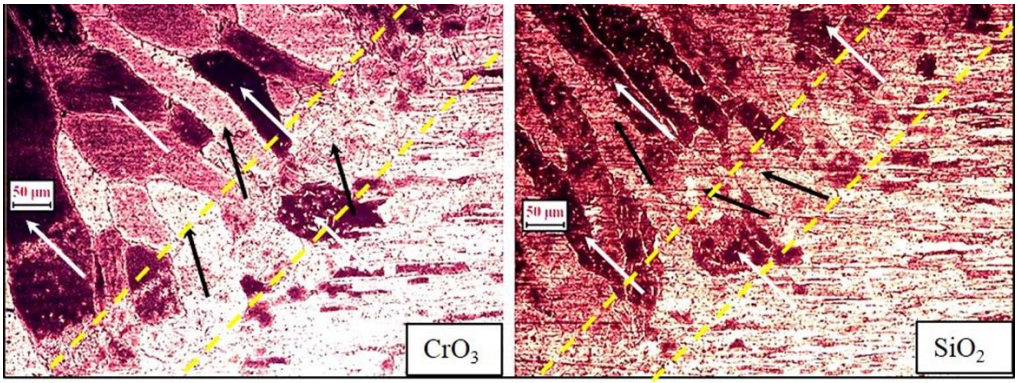

Figure 6. Optical micrograph of A-TIG welded samples under Ar + 2.5 % H_2 shielding

4.7. Peclet number analysis

The resulted weld pool profile and pool behaviour is influenced by the heat transfer rate which is based on the combined conduction & convection mode in the weld puddle and it may be different in different materials [13]. So, it is possible to investigate the mode of heat transfer based on Peclet number. The Peclet number calculation was suggested by Shanping Lu et.al. [2010]and may be calculated by $Pe = L*Vmax / 2\alpha l$ [10], [25], [26]. Where, V_{max} is the maximum surface velocity taken as 0.12 m/sec [25], [26],αl is the thermal diffusivity of liquid and L is the characteristic length or depth of the weld pool. The properties of duplex 2205 are taken as per the suggested values by Tathgir et.al. [10]. The Peclet number for CrO_3 flux in Ar shielding was found as 26.94 and in Ar + 2.5 % H2 shielding it was found as 26.84. Whereas in case of SiO_2 flux and in Ar shielding it was observed as 39.43 and for H_2 mix shielding it was observed as 26.63. Hence, from the study of Tathgir et. al. [10] we may say that the mode of heat transfer was dominated by convection mode, as the value of Peclet number is >> 1.

4.8. Micro-hardness analysis

The micro-hardness of the polished and etched specimens was conducted by applying the load of 500 gfwith holding time of 20 sec. An equal distance of 0.5 mm was maintained for the indentation. Hence, the micro-hardness ofA-TIG welded samples for short duration arc exposure time (2 sec) for different shielding environment are represented in Figure 7. The way of hardness measurement in horizontal (width direction of weld) and vertical (thickness direction of weld) regions also presented in the Figure 7. The indentation line for horizontal direction starts from the BM area and then passing through FZ area and then ended at BM area. The occurrence of different phases is depending on the variation in cooling rate, which further decide the micro-hardness value of that phase. This change of phase in the weld metal may affect the mechanical properties. The hardness variations could be a result of microstructure, which is mostly dendritic in nature.

Base metal micro-hardness was found to be approximately 262 HV. In case of Ar shielding, higher hardness values were obtained in case of SiO_2sample due to the presence of ferrite phase in the upper zone. But in case of Ar + 2.5 % H_2 shielding environment, the opposite trend was appeared. Higher hardness value was obtained in CrO_3 flux weld metal on the right-hand side of the graph which could be justified from the presence of ferrite phase on right hand side in Figure 2. However, the lower value was observed withthe sample welded with SiO_2 flux condition. Similar kind of variations with considerable variation in the hardness value was observedin thickness (vertical) direction measurement of the weld owing to mixed phase of dendritic structure.

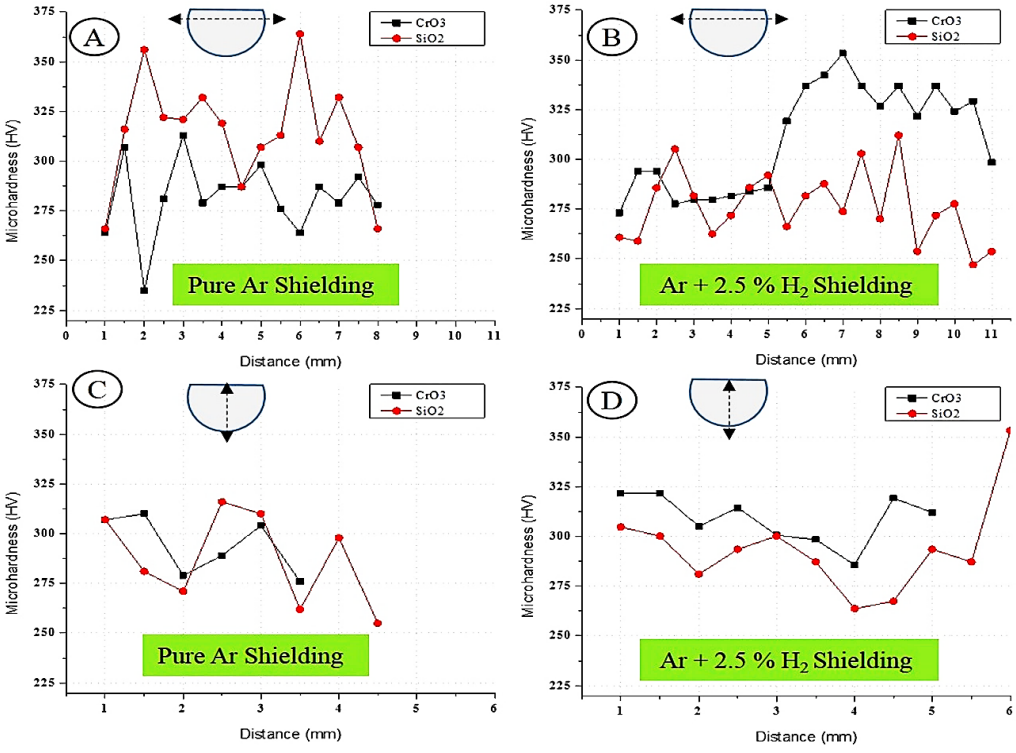

Figure 7. Micro-hardness comparison of A-TIG welded samples (A) & (B) for horizontal direction and (C) & (D) for vertical direction analysis

5. Conclusion

The significance of short weld time with Ar and Ar + 2.5% H_2 induced shielding environment by using oxygen rich fluxes i.e. CrO_3 and SiO_2 for A-TIG processes and the respective change in the microstructure has been investigated in the present study along with process phenomena. The perceived conclusions based on the experimental study and analysis have been summarized below.

- Dendrite growth rate and dendrite arm spacing is strongly influenced by the heat energy produced owing to oxygen element of the activated flux along with the H_2 induced shielding. The dendrites growth is found almost vertical in H_2 mixed shielding, whereas in case of Ar shielding it is at an angle of ~ 45° owing to the energy produces and associate cooling rate.
- The less percentage of hydrogen in argon is sufficient to increases the arc efficiency and decomposition of activated fluxes, which further produces high heat due to presence of oxygen element of flux. This is found to be significant in CrO_3 flux due to availability of more oxygen element and this further increases the Peclet number.
- Due to the attachment of electrons in the outer region of arc and redistribution the charge results into arc constriction with reduction of root area and the surface tension gradient become positive due to oxygen rich activated flux which further changes the metal flow in the centre of weld pool and finally promote deep penetration.
- Significant reduction in average austenite dendrite arm spacing as compared to ferrite dendrite arm spacing due to short duration of weld time and the associated cooling rate. However, the width of HAZ in Ar + 2.5 % H_2 shielding is found less as compared to pure Ar shielding.
- The average FGS and AGS for CrO_3 flux has been significantly increased during H_2 induced shielding than pure Ar shielding. However, the growth of AGS is found same in both the shielding environment in case of SiO_2 flux. Hence, the H_2 in shielding promotes the growth of ferrite than the austenite owing to higher electron affinity and reactions of H_2 with decomposed oxygen element.

In A-TIG welding with SiO_2 flux, due to effect of electron affinity toward silicon and the associated ferrite rich microstructure increases the hardness of weld metal, despite of variation in the cooling rate. This trend was not observed in H_2 mix shielding environment which consequently show the higher hardness value for CrO_3flux owing to more heat due to availability more oxygen molecules for the reaction with H_2.

Authors' Declaration

Authors' contributions and responsibilities - The authors made substantial contributions to the conception and design of the study. The authors took responsibility for data analysis, interpretation, and discussion of results. The authors read and approved the final manuscript.

Funding - No funding information from the authors.

Availability of data and materials - All data are available from the authors.

Competing interests - The authors declare no competing interest.

Additional information - No additional information from the athors.

References

[1] J. Rosado-Carrasco, U. Krupp, V. H. López-Morelos, A. Giertler, M. A. García-Rentería, and J. González-Sánchez, "Effect of a magnetic field applied during fusion welding on the fatigue damage of 2205 duplex stainless steel joints," *International Journal of Fatigue*, vol. 121, no. July 2018, pp. 243–251, 2019, doi: 10.1016/j.ijfatigue.2018.12.022.

[2] T. S. Chern, K. H. Tseng, and H. L. Tsai, "Study of the characteristics of duplex stainless steel activated tungsten inert gas welds," *Materials and Design*, vol. 32, no. 1, pp. 255–263, 2011, doi: 10.1016/j.matdes.2010.05.056.

[3] Z. M. Liu *et al.*, "Stable keyhole welding process with K-TIG," *Journal of Materials Processing Technology*, vol. 238, pp. 65–72, 2016, doi: 10.1016/j.jmatprotec.2016.07.005.

[4] Y. Shi, S. Cui, T. Zhu, S. Gu, and X. Shen, "Microstructure and intergranular corrosion behavior

of HAZ in DP-TIG welded DSS joints," *Journal of Materials Processing Technology*, vol. 256, no. November 2017, pp. 254–261, 2018, doi: 10.1016/j.jmatprotec.2018.02.019.

[5] D. Rathod, S. Aravindan, P. K. Singh, and S. Pandey, "Metallurgical characterization and diffusion studies of successively buttered deposit of Ni-fe alloy and inconel on SA508 ferritic steel," *ISIJ International*, vol. 54, no. 8, pp. 1866–1875, 2014, doi: 10.2355/isijinternational.54.1866.

[6] E. Folkhard, *Welding Metallurgy of Stainless Steels*. New York: Springer-Verlag/Wien, 1988.

[7] A. Bhattacharya, "Revisiting arc, metal flow behavior in flux activated tungsten inert gas welding," *Materials and Manufacturing Processes*, vol. 31, no. 3, pp. 343–351, 2016, doi: 10.1080/10426914.2015.1070421.

[8] S. Tathgir, A. Bhattacharya, and T. K. Bera, "Influence of Current and Shielding Gas in TiO2 flux Activated Tig Welding on Different Graded Steels," *Materials and Manufacturing Processes*, vol. 30, no. 9, pp. 1115–1123, 2015, doi: 10.1080/10426914.2014.973591.

[9] S. Tathgir and A. Bhattacharya, "Activated-TIG welding of different steels: Influence of various flux and shielding gas," *Materials and Manufacturing Processes*, vol. 31, no. 3, pp. 335–342, 2016, doi: 10.1080/10426914.2015.1037914.

[10] S. Tathgir, D. W. Rathod, and A. Batish, "A-TIG welding process for enhanced-penetration in Duplex stainless-steel: effect of activated fluxes," *Materials and Manufacturing Processes*, vol. 34, no. 15, pp. 1659–1670, Nov. 2019, doi: 10.1080/10426914.2019.1666990.

[11] A. Kulkarni, D. K. Dwivedi, and M. Vasudevan, "Effect of oxide fluxes on activated TIG welding of AISI 316L austenitic stainless steel," in *Materials Today: Proceedings*, 2019, vol. 18, pp. 4695–4702, doi: 10.1016/j.matpr.2019.07.455.

[12] S. Tathgir, D. W. Rathod, and A. Batish, "Process enhancement using hydrogen-induced shielding: H2-induced A-TIG welding process," *Materials and Manufacturing Processes*, vol. 35, no. 10, pp. 1084–1095, 2020.

[13] S. Lu, H. Fujii, and K. Nogi, "Weld shape variation and electrode oxidation behavior under Ar-(Ar-CO2) double shielded GTA welding," *Journal of Materials Science and Technology*, vol. 26, no. 2, pp. 170–176, 2010, doi: 10.1016/S1005-0302(10)60028-X.

[14] S. Tathgir and A. Bhattacharya, "Activated-TIG welding of different steels: Influence of various flux and shielding gas," *Materials and Manufacturing Processes*, vol. 31, no. 3, 2016, doi: 10.1080/10426914.2015.1037914.

[15] J. J. Lowke, M. Tanaka, and M. Ushio, "Mechanisms giving increased weld depth due to a flux," *Journal of Physics D: Applied Physics*, vol. 38, no. 18, pp. 3438–3445, 2005, doi: 10.1088/0022-3727/38/18/018.

[16] M. Suban, J. Tušek, and M. Uran, "Use of hydrogen in welding engineering in former times and today," *Journal of Materials Processing Technology*, vol. 119, no. 1–3, pp. 193–198, 2001, doi: 10.1016/S0924-0136(01)00956-6.

[17] D. W. Rathod, S. Pandey, S. Aravindan, and P. K. Singh, "Diffusion Control and Metallurgical Behavior of Successive Buttering on SA508 Steel Using Ni–Fe Alloy and Inconel 182," *Metallography, Microstructure, and Analysis*, vol. 5, no. 5, pp. 450–460, 2016, doi: 10.1007/s13632-016-0311-z.

[18] K. H. Tseng and P. Y. Chen, "Effect of TiO2 crystalline phase on performance of flux assisted GTA welds," *Materials and Manufacturing Processes*, vol. 31, no. 3, pp. 359–365, 2016, doi: 10.1080/10426914.2015.1058952.

[19] E. Ahmadi and A. R. Ebrahimi, "Welding of 316L Austenitic Stainless Steel with Activated Tungsten Inert Gas Process," *Journal of Materials Engineering and Performance*, vol. 24, no. 2, pp. 1065–1071, 2014, doi: 10.1007/s11665-014-1336-6.

[20] J. J. Vora and V. J. Badheka, "Experimental investigation on mechanism and weld morphology of activated TIG welded bead-on-plate weldments of reduced activation ferritic/martensitic steel using oxide fluxes," *Journal of Manufacturing Processes*, vol. 20, pp. 224–233, 2015, doi: 10.1016/j.jmapro.2015.07.006.

[21] Y. L. Xu, Z. B. Dong, Y. H. Wei, and C. L. Yang, "Marangoni convection and weld shape variation in A-TIG welding process," *Theoretical and Applied Fracture Mechanics*, vol. 48, no. 2, pp. 178–186, 2007, doi: 10.1016/j.tafmec.2007.05.004.

[22] K.-H. Tseng and K.-L. Chen, "Comparisons between TiO2-and SiO2- Flux Assisted TIG Welding Processes.," *Journal of Nanoscience and Nanotechnology*, vol. 12, no. 8, pp. 6359–6367, 2012, doi: 10.1166/jnn.2012.6419.

[23] S. Kou, *Welding Metallurgy*, Second. New Jersey: A John Wiley & Sons, Inc., Publication, 2003.

[24] R. Blondeau, *Metallurgy and Mechanics of Welding: Processes and Industrial Applications*. New Jersey: A John Wiley & Sons, Inc., Publication, 2010.

[25] T. Zacharia, S. A. David, J. M. Vitek, and T. Debroy, "Weld Pool Development during GTA and Laser Beam Welding of Type 304 Stainless Steel , Part I — Theoretical Analysis," *Weld. J. Res. Suppl.*, vol. 68, no. 12, p. 499s To 509s, 1989.

[26] T. Zacharia, S. A. David, J. M. Vitek, and T. Debroy, "Weld Pool Development during GTA and Laser Beam Welding of Type 304 Stainless Steel , Part II — Experimental Correlation," *Weld. J. Res. Suppl.*, vol. 68, no. 12, pp. 510s-520s, 1989.